Assembly history of the Magellanic Bridge and Small Magellanic Cloud Wing from star clusters

PhD Thesis by Raphael Oliveira

Thesis goals

- age and metallicity analysis of Wing and Bridge star clusters to help distinguish between two scenarios for the Magellanic System history:
  - the Magellanic Clouds were independent satellites and got bound recently, at ~ 2 Gyr ago; had 2 encounters since then at 1.2 Gyr and 250 Myr ago (Diaz & Bekki 2011)
  - the Magellanic System is old and on its first passage across the Milky Way in the last ~ 2 Gyr; recent frontal encounter at 200-300 Myr ago (Besla et al. 2012)

--» homogeneous analysis of the Bridge (both data and methods)

Data

- VISCACHA „VIsible Soar photometry of star Clusters in tApii and Coxi HuguA”
- SMASH „Survey of the MAgellanic Stellar History”

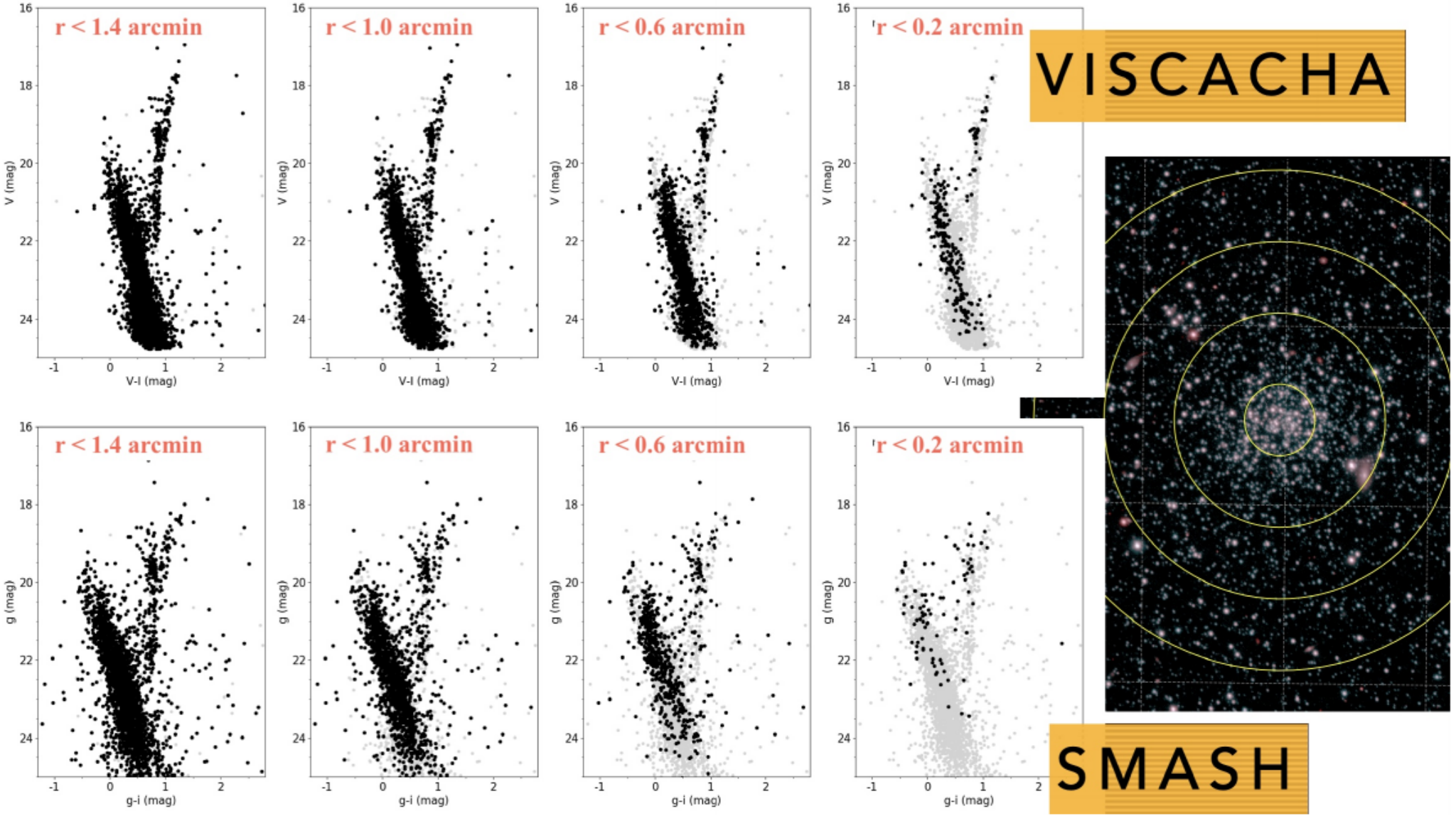
r < 1.4 arcmin
r < 1.0 arcmin
r < 0.6 arcmin
r < 0.2 arcmin
V (mag)
V-I (mag)
g (mag)
g-i (mag)
VISCACHA
SMASH

The statistical analysis

1. Cluster parameters from the distribution of stars
2. Cleaning the data from non-cluster members
3. Fundamental parameters from CMDs

1. Cluster parameters from the distribution of stars

- The King profile (King 1962) reproduces cluster radial density profile (RDP) with structural parameters:
  - r_t – tidal radius (zero surface density)
  - r_c – core radius (density drops by half)
  - ρ_0 – central surface density
  - ρ_{bg} – density of background stars
  - $\rho(r)$ – predicted stellar density at distance r

$$\rho(r) = \rho_0 \left[\frac{1}{\sqrt{1+(r/r_c)^2}} - \frac{1}{\sqrt{1+(r_t/r_c)^2}} \right]^2 + \rho_{\rm bg} \ , \qquad (3.1)$$

1. Cluster parameters from the distribution of stars

- RO developed a Python code from scratch to produce RDP, followed by a statistical fitting of King empirical models on the RDP to obtain the structural parameters
- new approach to estimating density vs radius:
  evaluate the density around each of the N stars retrieved in the photometry, using a circle (in the RA-Dec plane) with an adaptive radius R_i that contains $\sqrt{N}$ stars, through $\rho_i = \sqrt{N} / (\pi \cdot R_i^2)$

1. Cluste … of stars

- RO deve … RDP, followed … on the RDP to c…
- new app … ed in the evaluate … n adaptive photome… radius R…

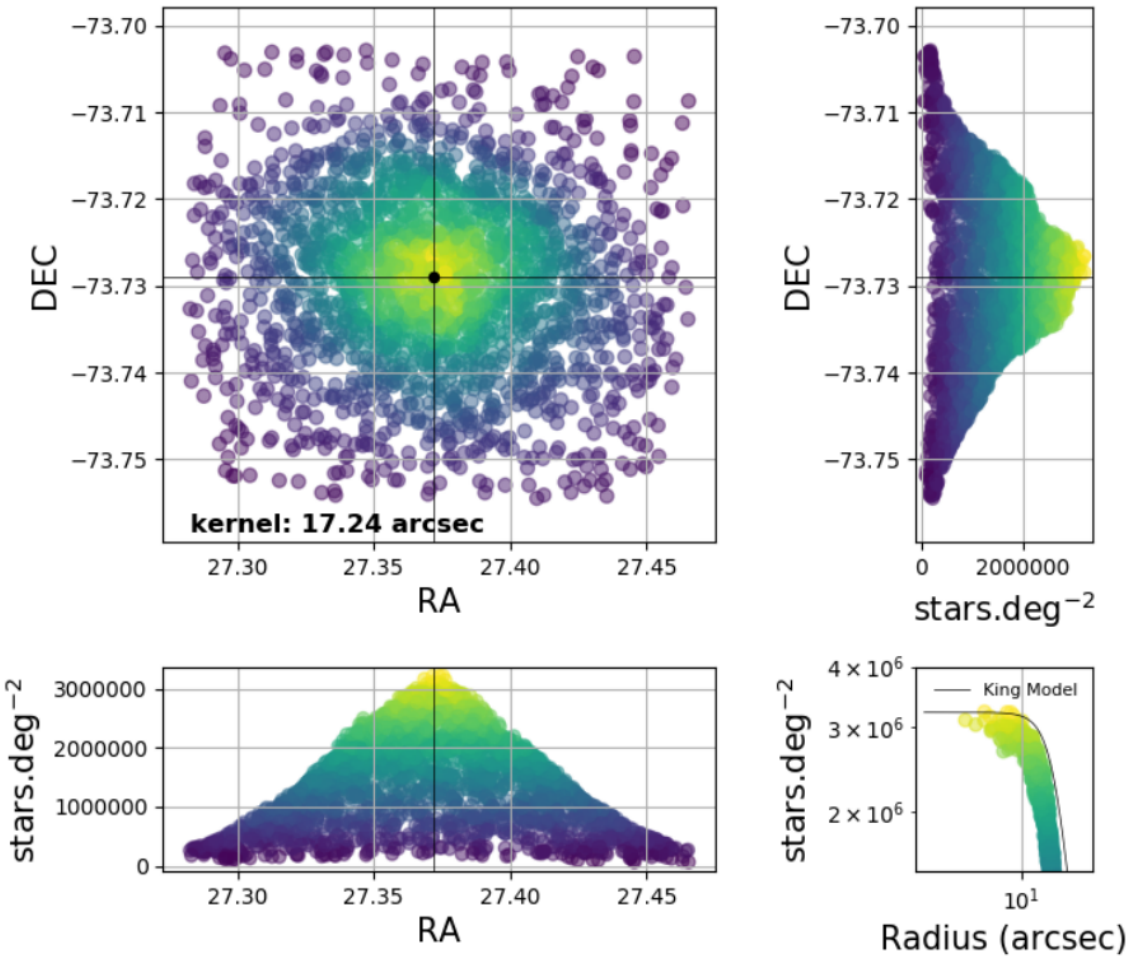

Figure 3.1: Layout of the method implemented to generate the radial density profile (lower right panel). The upper left panel presents the equatorial coordinates of all N stars detected in the photometry of L113, each star with a local calculation of the density in a circle containing $\sqrt{N}$ stars. The other two panels present the 1D projections in each coordinate.

1. Cluster parameters from the distribution of stars

- parameter determination is based on a likelihood function together with the MCMC method, with 6 independent random walkers:
  α_{cen} , δ_{cen} , r_t , r_c , ρ_0 , ρ_{bg}
- maximize the probability that a given King model represents the distribution of stellar densities as a function of the radius in the RDP
- 6D parameter space is sampled with the emcee package (“The MCMC Hammer”; Foreman-Mackey et al., 2013)

1. Cluster parameters from the distribution of stars

$$L_i = \exp(-\chi_i^2) \propto \exp\left[-\frac{(\rho_{i,data} - \rho_{j,model})^2}{2\sigma_{i,data}^2}\right] , \tag{3.3}$$

where $\rho_{i,data}$ is the density around the star i, $\rho_{j,model}$ is the density predicted by the tentative King model at the radius r, and $\sigma_{i,data}$ is the statistical Poissonian error of each density estimation, i.e. $\sigma_{i,data} = \sqrt{N}/(\pi \cdot R_i^2)$. The final likelihood of a tentative model is given by the natural logarithm of the product with the contribution of all N stars:

$$\mathcal{L} = \ln \prod_{i=1}^{N} L_i = \sum_{i=1}^{N} \ln(L_i) \propto \sum_{i=1}^{N} \left[-\frac{(\rho_{i,data} - \rho_{j,model})^2}{2\sigma_{i,data}^2}\right] . \tag{3.4}$$

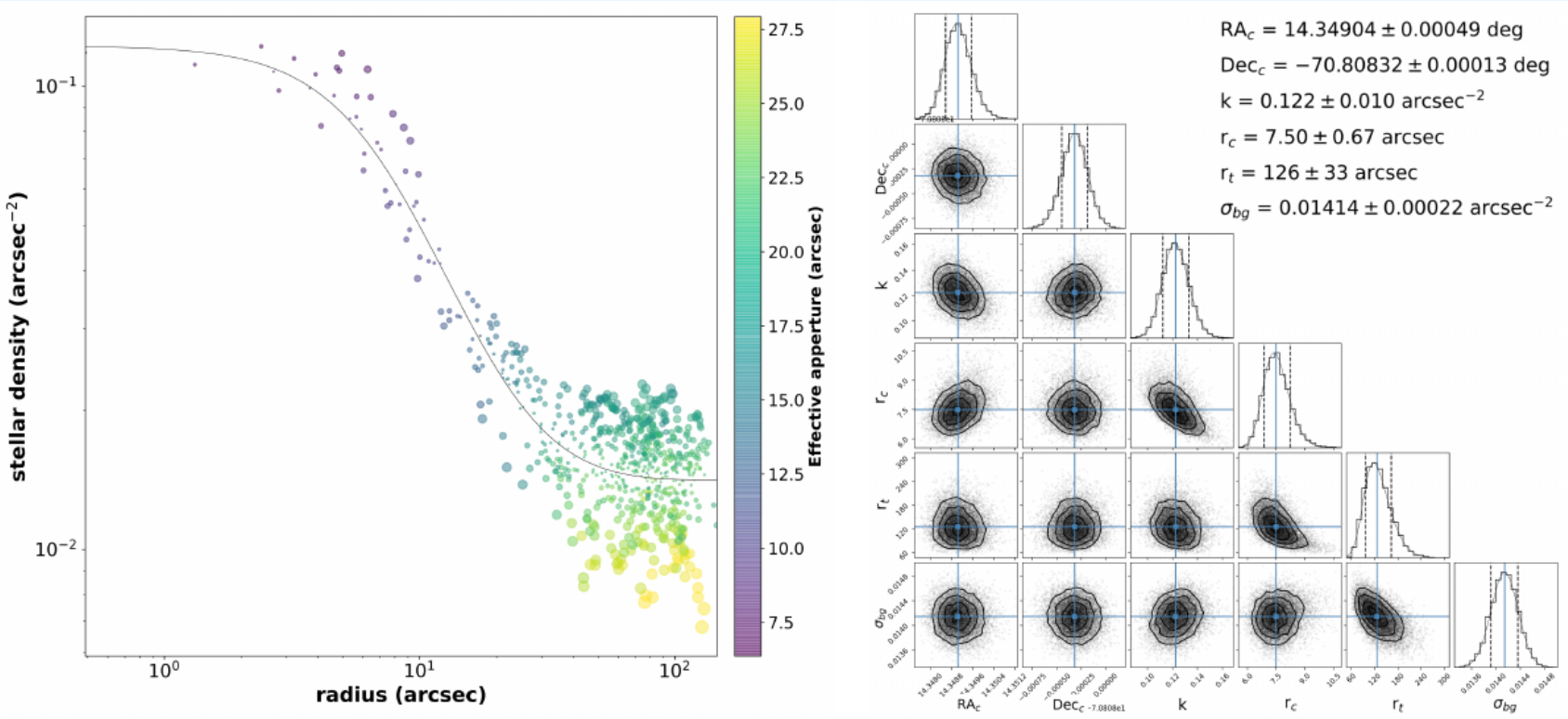

Figure 3.2: (Left:) Radial density profile of HW33 with the best fit King model, colour-coded by the aperture size necessary to include $\sqrt{N}$ stars. *(Right:)* Corner plots with the posterior probability distributions obtained from MCMC. The diagonal panels show the posterior for the six free parameters, and the remaining ones show the correlations between each two parameters. A skewed gaussian is fitted to each histogram to account for distributions with tails, and the corresponding solution and 1σ is given in the upper right. The dashed lines correspond to the 16 and 84th percentiles.

1. Cluster n of stars

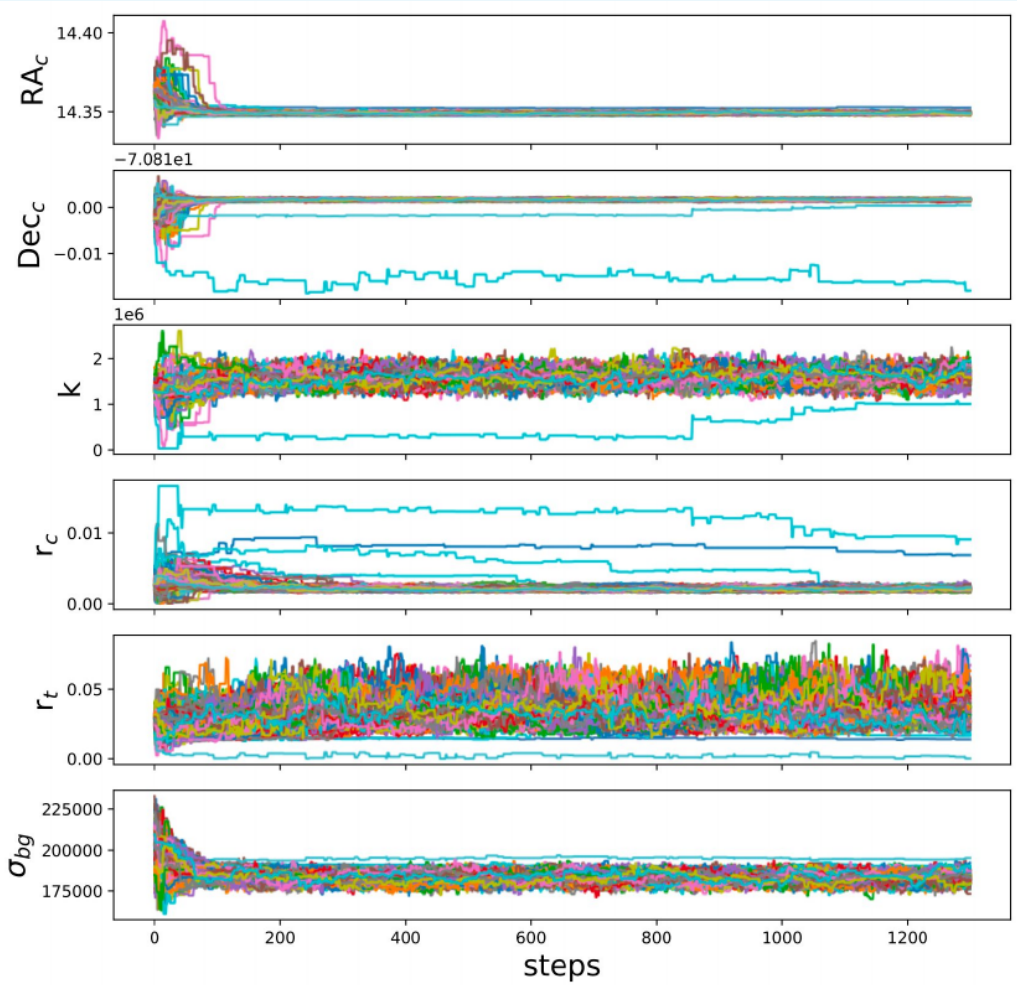

Figure 3.3: Tracer plots showing the evolution of the convergence of walkers in the simulated chains for HW33 (same as Figure 3.2). Each panel shows the convergence for each parameter, whereas each line corresponds to an independent walker. In this case, the convergence of the walkers (related to the autocorrelation time) is reached with 1300 steps.

2. Cleaning the data from non-cluster members

- field stars
- crowding
- interstellar reddening
- large distances

2. Cleaning the data from non-cluster members

- **field stars**
- ~~crowding~~ AO
- ~~interstellar reddening~~ AO
- ~~large distances~~ AO

2. Cleaning the data from non-cluster members

- improved photometric method (from positions and magnitudes) developed by Maia et al. (2020)
- two regions: $r > r_t$ (field sample) and $r < r_t$ (field+cluster sample)
- star by star comparison based on the photometric similarity of the star with the nearby field, and on its distance from the centre
- assigning a membership probability value depending on the overdensity around the star position in the cluster and field CMDs
- RO inserted more constraints, such as the density around each star as an additional constraint when comparing the cluster with the field sample, and rewrote the entire code in Python

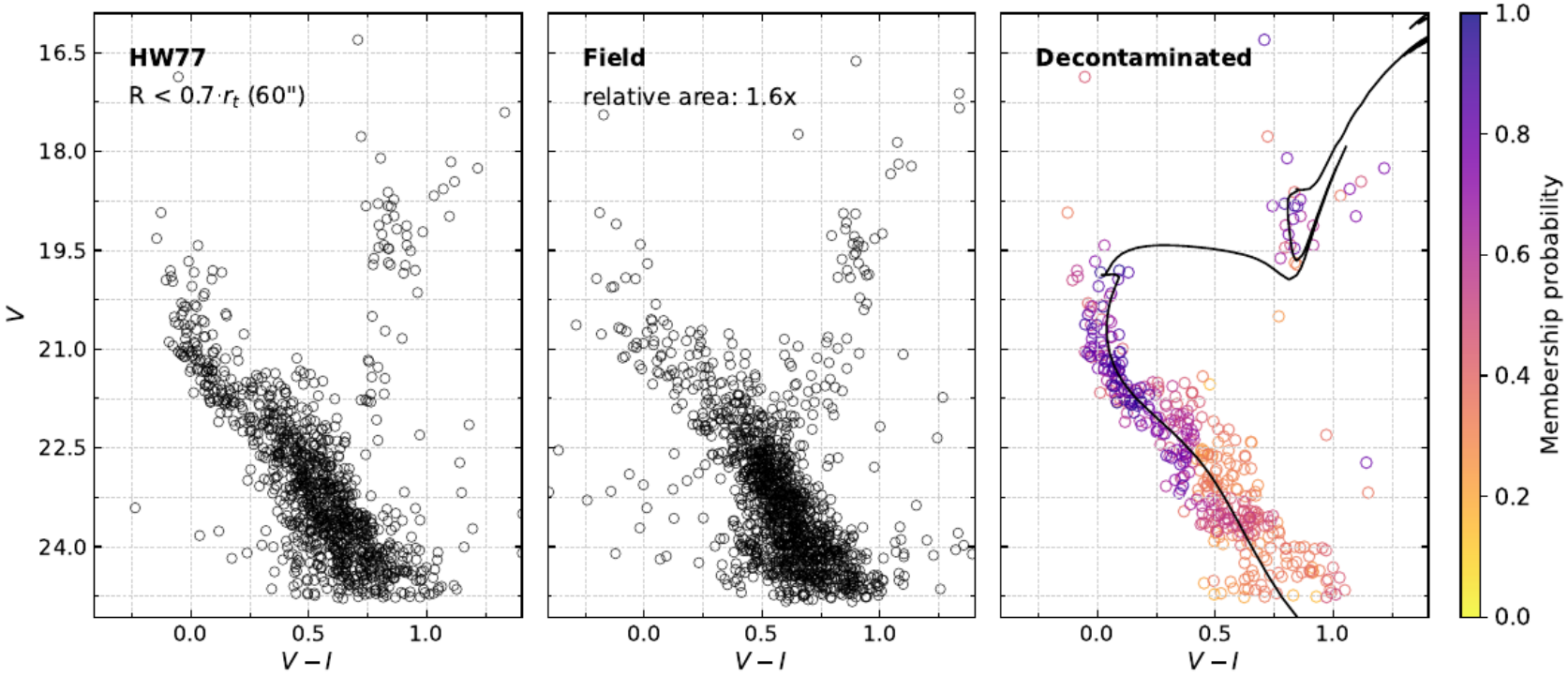

Figure 3.4: V vs. $V - I$ CMDs for the SMC Wing/Bridge cluster HW77 with VISCACHA data, showing the inputs and the output of the statistical decontamination method. *(Left:)* Initial CMD with the stars inside 60 arcsec (i.e. 70% of the derived tidal radius). *(Middle:)* Initial CMD with all the stars outside the tidal radius, with a relative area 1.6 greater than that of the first CMD. *(Right:)* Final decontaminated CMD, colour-coded by the membership probability and with a PARSEC isochrone of ~ 1 Gyr overlaid.

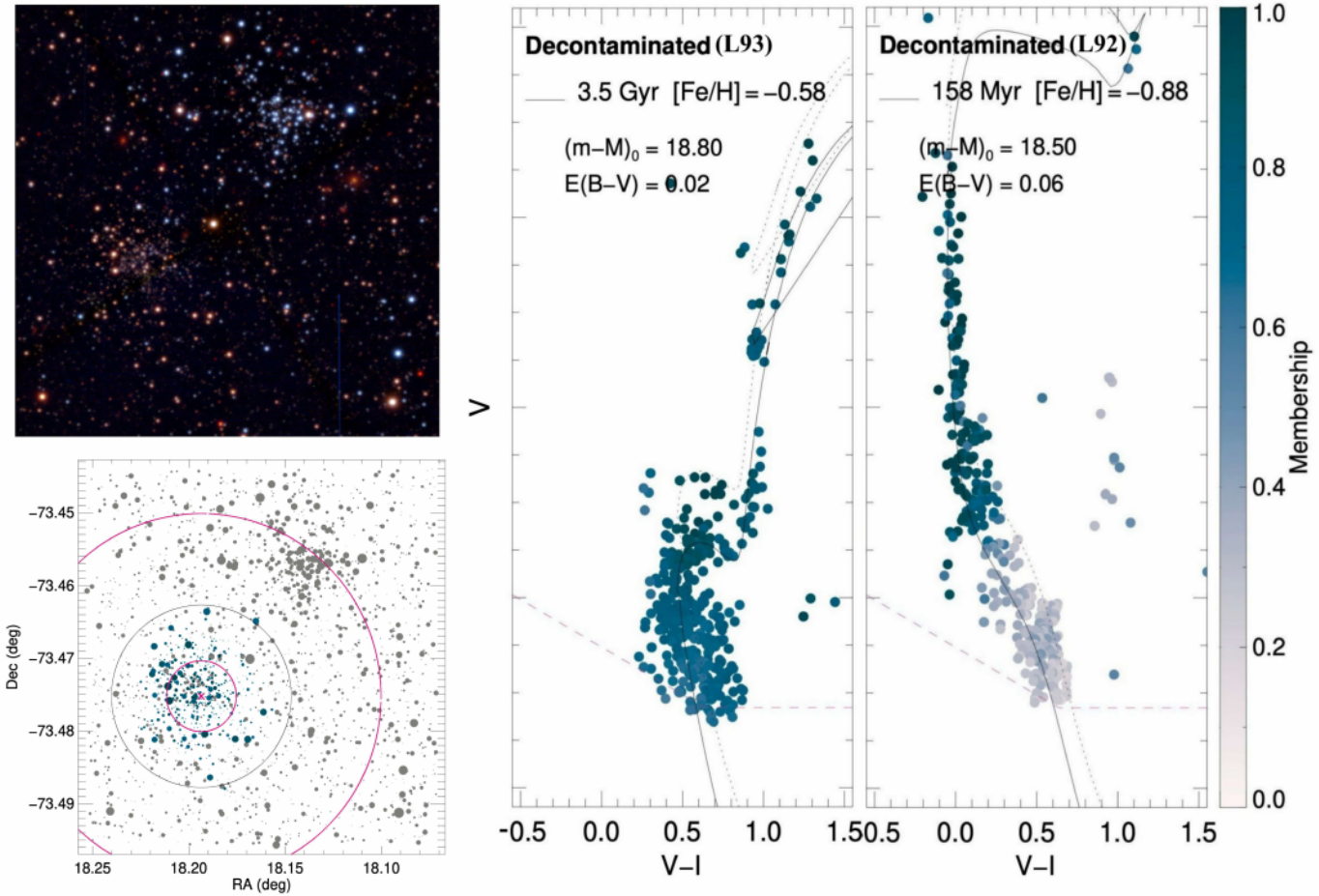

Figure 3.5: Decontamination process for the pair L92+L93, inside the same SAMI field of $3 \times 3\,\mathrm{arcmin}^2$ (upper left). The lower left panel shows the core and tidal radii of L93 as pink circles, and the assumed radius for the cluster sample ($0.5r_t = 47''$) in black. The two CMDs show the decontaminated photometry for the clusters, with a visual isochrone fit.

3. Fundamental parameters from CMDs

- set of isochorones (e.g. PARSEC,DSED, BaSTI) to reproduce the observed distribution in color and magnitude, in a sequence of simulated masses
- distribution of birth masses from the IMF (Kroupa 2001)
- includes distance moduli and reddening to move from HR to CMD

3. Fundamental parameters from CMDs

For a generic CMD λ_1 vs. $\lambda_1 - \lambda_2$,

the isochrone is shifted down by an apparent distance modulus $(m - M)_{\lambda_1}$ value, which is transformed to absolute distance modulus and heliocentric distance by:

$$(m - M)_0 = (m - M)_{\lambda_1} - \frac{A_{\lambda_1}}{A_V} \cdot R_V \cdot E(B - V) \tag{3.5}$$

$$d_\odot[\mathrm{kpc}] = 10^{[(m-M)_0 - 10]/5} , \tag{3.6}$$

where A_{λ_1}/A_V is the extinction coefficient[4] for the λ_1 filter and $R_V = A_V/E(B-V) \sim 3.1$ is the total-to-selective extinction ratio (Cardelli et al., 1989). The horizontal shift to the right is given by the reddening $E(\lambda_1 - \lambda_2)$, which relates to $E(B - V)$ through:

$$E(\lambda_1 - \lambda_2) = R_V \cdot E(B - V) \cdot \left[\frac{A_{\lambda_1}}{A_V} - \frac{A_{\lambda_2}}{A_V} \right] . \tag{3.7}$$

3. Fundamental parameters from CMDs

- set of isochorones (e.g. PARSEC,DSED, BaSTI) to reproduce the observed distribution in color and magnitude, in a sequence of simulated masses
- distribution of birth masses from the IMF (Kroupa 2001)
- includes distance moduli and reddening to move from HR to CMD

---> simultaneous fitting of age, metallicity, distance modulus and reddening

3. Fundamental parameters from CMDs

- SIRIUS code “Statistical Inference of physical paRameters of sIngle and mUltiple populations in Stellar clusters”, developed by the group

$$L_i \propto \exp\left[-\frac{(mag_j - mag_i)^2}{2\sigma_{mag}^2}\right] \cdot \exp\left[-\frac{(col_j - col_i)^2}{2\sigma_{col}^2}\right] , \tag{3.8}$$

where the indices i and j correspond to each star and isochrone point, respectively, and σ_{mag} and σ_{col} are the photometric errors. The total likelihood $\mathcal{L}$ is obtained summing the contribution of each star i (out of a total of N) compared to the color and magnitude of the j-th isochrone point closer to this star (obtained with a max function):

$$\mathcal{L} \propto \sum_{i=1}^{N} \max\left[-\sum_{j=1}^{M} \frac{(mag_j - mag_i)^2}{2\sigma_{mag}^2} + \frac{(col_j - col_i)^2}{2\sigma_{col}^2}\right] . \tag{3.9}$$

3. Fundamental parameters from CMDs

RO input includes:

- adapting SIRIUS code to work with PARSEC isochrones covering a larger age range than those adopted for Galactic GCs
- incorporating improvements for better fitting young and intermediate-age clusters, such as:
  - modifications in the likelihood function (e.g. membership probability p_{memb} and number of neighbour stars n_* on the CMD)
  - pre-selection of stars and priors based on the MSTO and red clump position to better constrain the posterior $P(\Phi)$.

3. Fundamental parameters from CMDs

RO input includes:

- adapting SIRIUS code to work with PARSEC isochrones covering a larger age range than those adopted for Galactic GCs
- incorporating improvements for better fitting young and intermediate-age clusters, such as:
  - modifications in the likelihood function (e.g. membership probability p_{memb} and number of neighbour stars n_* on the CMD)
  - pre-selection of stars and priors based on the MSTO and red clump position to better constrain the posterior $P(\Phi)$.

$$\mathcal{L} \propto \sum_{i=1}^{N} \left[-\chi^2_{\mathrm{mag,i}} - \chi^2_{\mathrm{col,i}} + \ln(p_{memb,i}) - \ln(n_*) \right] + P(\phi) \ . \qquad (3.10)$$

3. Fundamental parameters from CMDs

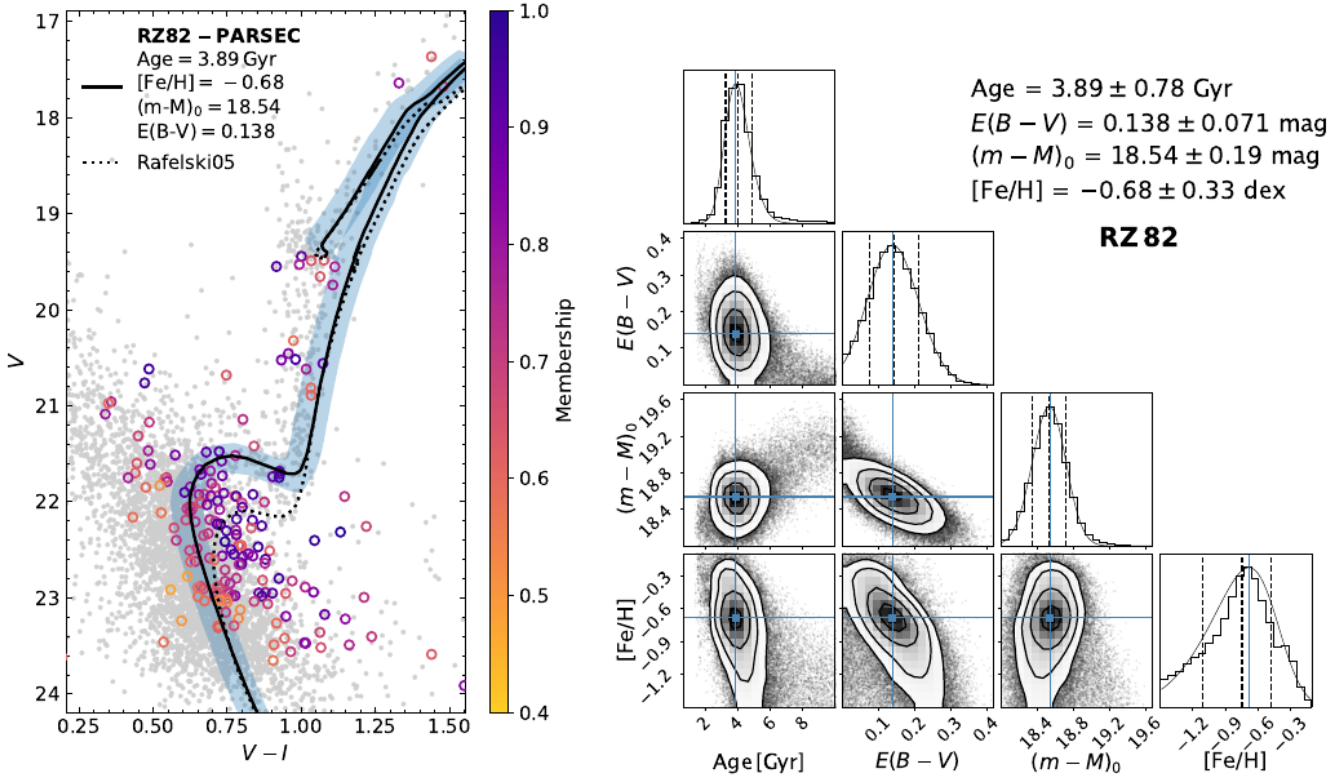

Figure 3.7: Results obtained with the SIRIUS code for the cluster RZ 82, with VISCACHA data (Bica et al. 2022). *(Left:)* Best-fitting PARSEC isochrone in the observed CMD, with a shaded region representing the solutions within 1σ. *(Right:)* Corner plot with the posterior distributions in the free parameters (age, metallicity, distance modulus and reddening).

Results for 33 clusters from VISCACHA

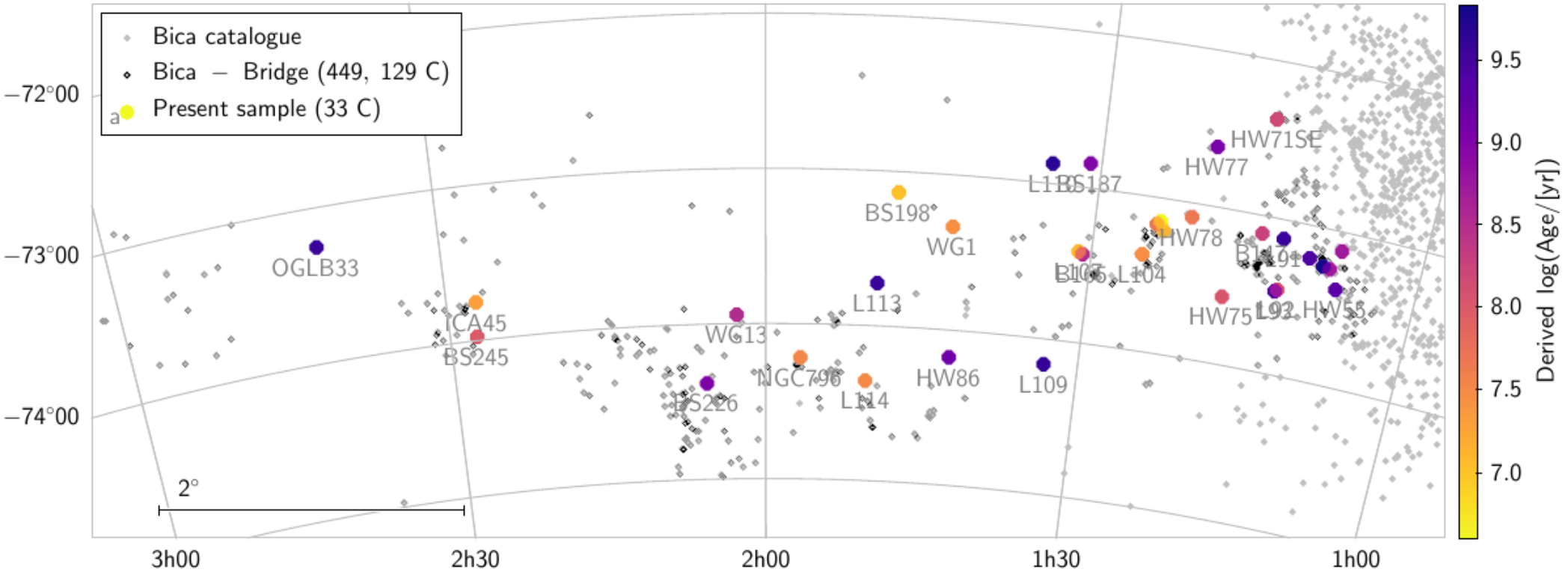

Results for 33 clusters from VISCACHA

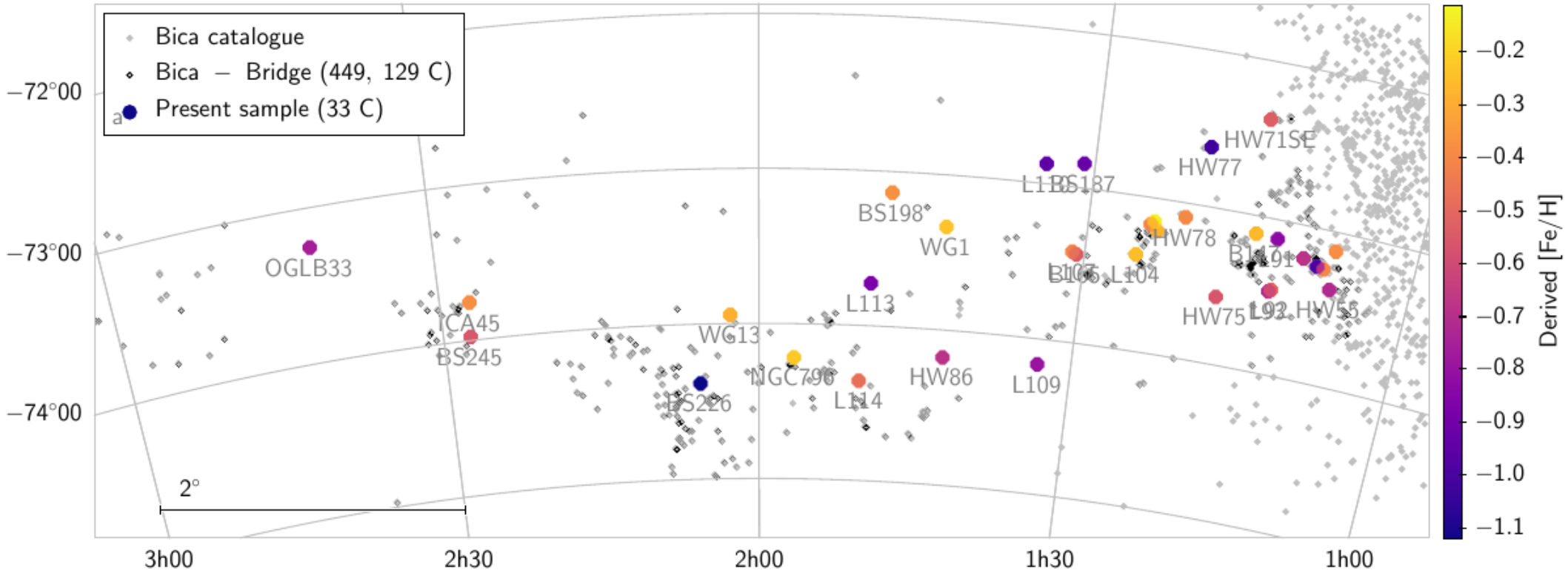

Results for 33 clusters from VISCACHA

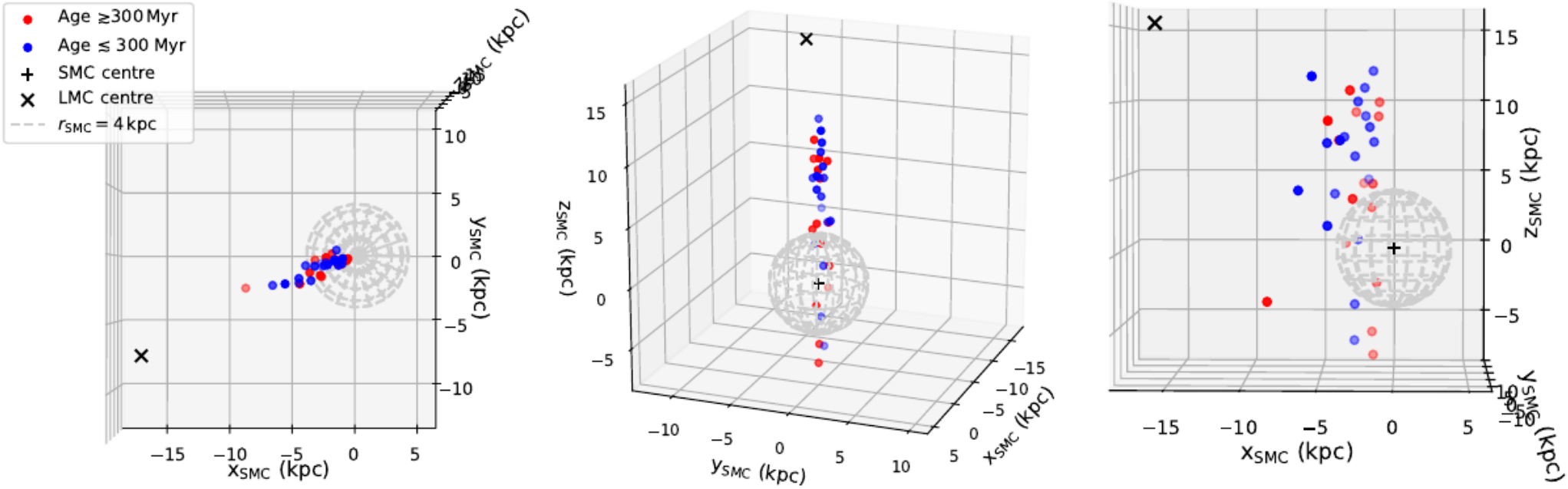

Figure 4.6: Three-dimensional distribution of the 33 sample clusters, identifying the old and the young clusters in red and blue: *(left:)* x vs. y similar to the sky projection; *(middle:)* projection showing the alignment between SMC, LMC and Bridge clusters with different depth; *(right:)* x vs. z projection. The SMC is located at the origin, the LMC is at $(x, y, z) = (-16.0, -7.2, 15.2)$, and the sphere corresponds to the SMC tidal radius of 4 kpc.

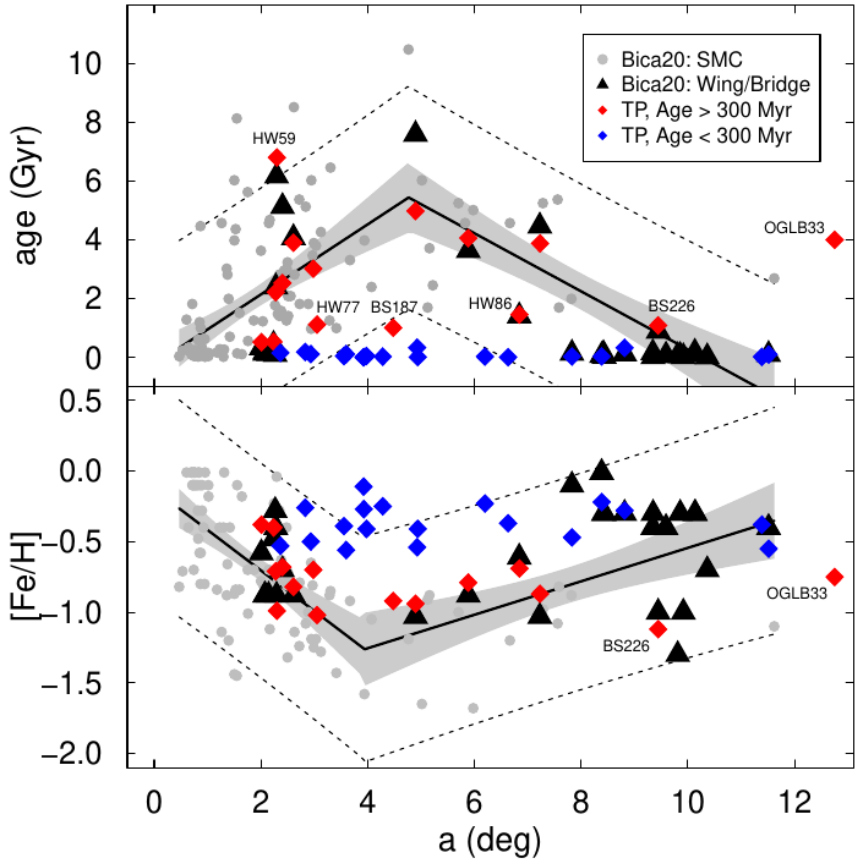

Figure 4.7: Derived age and metallicity as a function of the projected distance to the SMC centre. The grey and black symbols are from Bica et al. (2020), and the red and blue diamonds are the present sample of old and young clusters. The solid and dashed lines and the grey shaded areas represent the fit to the Bica et al. (2020) age and metallicity distributions as detailed in that work. It is clear that the old clusters follow the overall SMC gradients (exception are annotated) and the young ones have very similar metallicities.

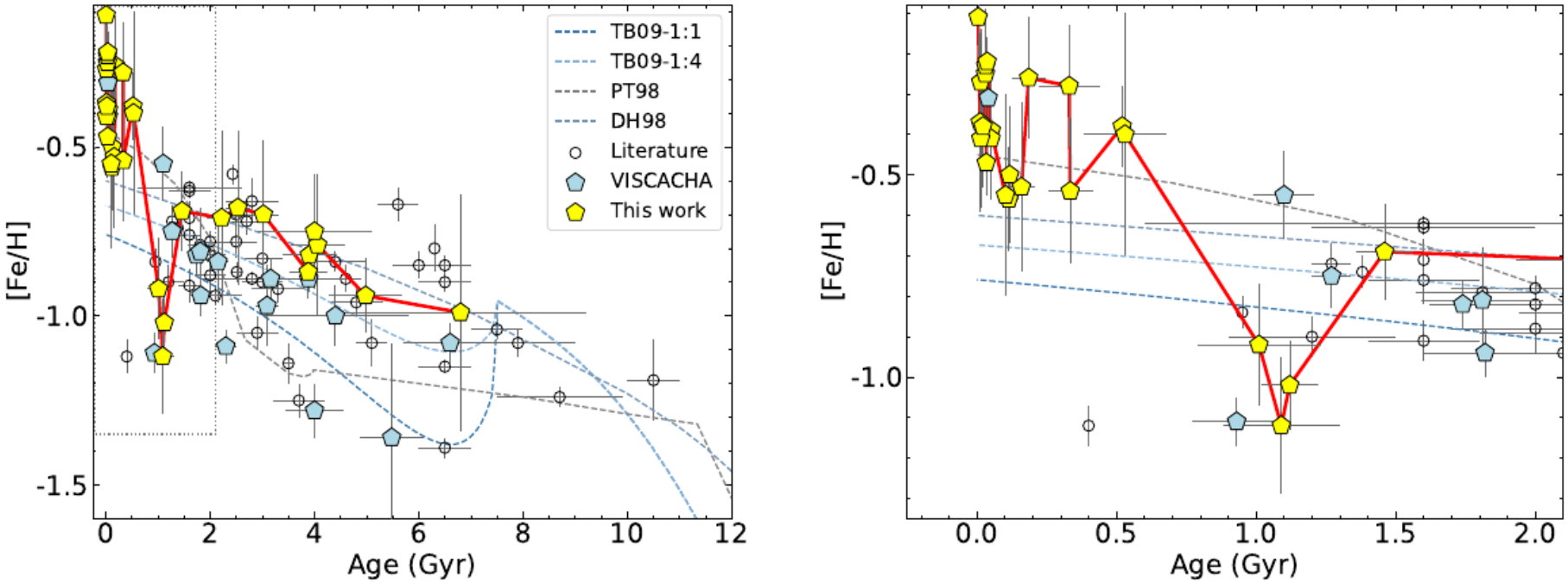

Figure 4.8: Age-metallicity relation of the present results for the Wing/Bridge clusters (yellow pentagons), previous results from VISCACHA (blue pentagons) and literature data with CaT metallicities (open black circles). Chemical evolution models are overplotted: Pagel and Tautvaisiene (1998, PT98), Da Costa and Hatzidimitriou (1998, DH98) and Tsujimoto and Bekki (2009, TB09). A red line connects the results from the older to the younger cluster, suggesting the existence of a large dip around $1 - 1.5$ Gyr and smaller one around 200 Myr. The right panel shows a zoom-in of < 2 Gyr.

Side project – bulge RR Lyrae in clusters

- having metallicity and reddening for a cluster with RRL. its distance can be determined from PLZ relation for RRL
- 6 bulge clusters with RRL from OGLE-IV and PMs from Gaia DR3
- 2D Gaussian mixture models were used to identify two distributions in the PM space (cluster distribution has a lower dispersion)
- RR Lyrae membership probability was calculated based on RRL, cluster and field PMs and uncertainties

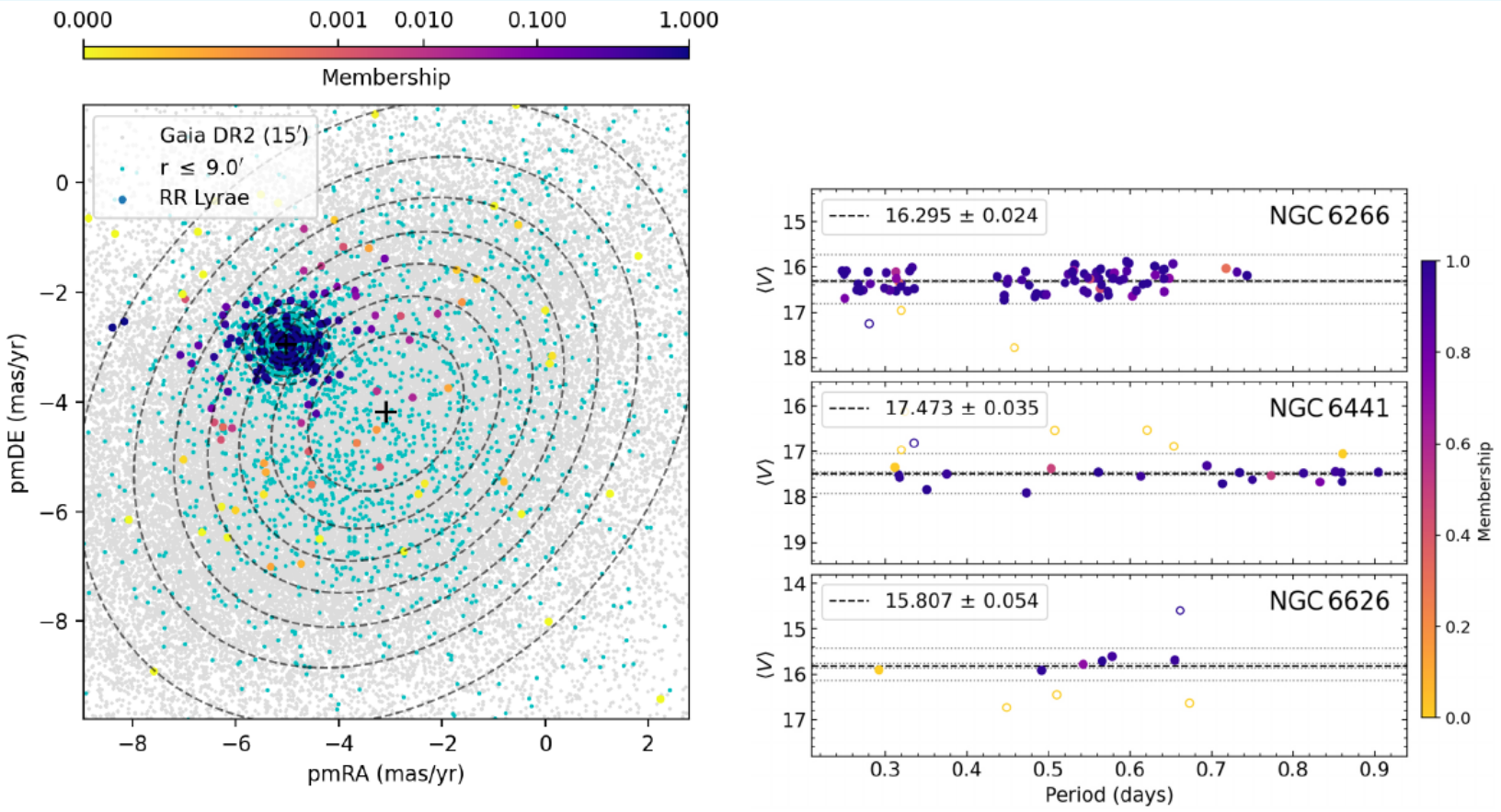

Figure 5.3: *(Left:)* Proper motions diagram of NGC 6266, showing the 242 RRLs colour-coded by the derived memberships, and the two Gaussian distributions (cluster and field), derived from the two-dimensional GMM. *(Right:)* Mean V magnitudes (Clement et al., 2001) of three clusters versus period of pulsation, where the dashed lines represent the average and the 2σ level, used to calculate the distance.

Side project – bulge RR Lyrae in clusters

- from RRL mean magnitudes, new M_λ − [Fe/H] relations were constructed, using updated BaSTI models for the zero-age horizontal branch
- RO obtained distances of:

  6.6 kpc, 13.1 kpc, 5.6 kpc, 9.6 kpc, 8.2 kpc and 7.3 kpc for NGC 6266, NGC 6441, NGC 6626, NGC 6638, NGC 6642, and NGC 6717 with 5−6% precision